Delft University of Technology

Delft Center for Systems and Control

Technical report 12-004

Modeling, analysis, and simulation of a cryogenic distillation process for ^{13}C isotope separation*

D.C. Dumitrache, B. De Schutter, A. Huesman, and E. Dulf

If you want to cite this report, please use the following reference instead:
D.C. Dumitrache, B. De Schutter, A. Huesman, and E. Dulf, "Modeling, analysis, and simulation of a cryogenic distillation process for ^{13}C isotope separation," *Journal of Process Control*, vol. 22, no. 4, pp. 798–808, Apr. 2012.

Delft Center for Systems and Control
Delft University of Technology
Mekelweg 2, 2628 CD Delft
The Netherlands
phone: +31-15-278.51.19 (secretary)
fax: +31-15-278.66.79
URL: `http://www.dcsc.tudelft.nl`

*This report can also be downloaded via `http://pub.deschutter.info/abs/12_004.html`

Modeling, Analysis, and Simulation of a Cryogenic Distillation Process for ^{13}C Isotope Separation

Dan Călin Dumitrache[a,b,*], Bart De Schutter[a], Adrie Huesman[a], Eva Dulf[b]

[a] *Delft Center for Systems and Control, Delft University of Technology, Mekelweg 2, 2628 CD Delft, The Netherlands*
[b] *Department of Automatic Control, Technical University of Cluj-Napoca, G. Baritiu 26-28, 400027, Cluj-Napoca, Romania*

Abstract

This paper presents a structured and insightful approach to modeling and simulation of an isotopic enrichment plant that uses distillation principles for ^{13}C isotope separation. First, after a brief review of distillation and mass transfer-related topics, a full nonlinear model for the cryogenic distillation process for ^{13}C isotope separation is derived from first-principles knowledge. In order to derive the mathematical description of the concerned isotope separation process, based on the two-film theory, we will derive the rate of transfer of the ^{13}C isotope from the vapor phase to the liquid phase. Since the isotope separation by cryogenic distillation is usually carried out in a very long column with a small diameter, a good approximation arises by neglecting the radial diffusion. We continue with the determination of the system of the partial differential equations that governs the evolution of desired isotope during the separation process. Next, we solve the system of partial differential equations, resulting in the full nonlinear model. Due to the complexity of the full nonlinear model, we consider two additional alternative modeling approaches resulting in a quasi-linear model and, when the isotope concentration achieved is low, a linear approximation model. In the second part of the paper we use the finite-differences method for the numerical analysis and numerical simulation of the three models, followed by the assessment of the linear model for future tasks in modeling, optimization, and process control.

Keywords:
Isotope separation, Cryogenic distillation, Modeling, Distributed parameter system, Numerical analysis, Simulation

1. Introduction

Isotopes of various elements have different applications in a variety of fields such as hydrology, geology, and medicine [1, 2, 3]. Some of these applications have a basis in techniques like determining the isotopic signature of an investigated material or the use of labeled compounds for tracing them from one part of a system to another. These techniques provide information used in studying e.g.

*Corresponding author. Tel.: +40 740 365 167; Fax: +40 266 313 058;
E-mail address: dan.dumitrache@aut.utcluj.ro

	Latin symbols	
A	area	m^2
c	molar concentration	$\frac{\mathrm{mol}}{\mathrm{m}^3}$
d	diameter	m
D	molecular diffusivity	$\frac{\mathrm{m}^2}{\mathrm{s}}$
h	height	m
H	hold-up per unit volume	$\frac{\mathrm{mol}}{\mathrm{m}^3}$
HETP	height equivalent to a theoretical plate	m
J	molar flux	$\frac{\mathrm{mol}}{\mathrm{m}^2\mathrm{s}}$
K	volumetric overall mass transfer coefficient	$\frac{\mathrm{mol}}{\mathrm{m}^3\mathrm{s}}$
L	liquid molar flow rate per unit area	$\frac{\mathrm{mol}}{\mathrm{m}^2\mathrm{s}}$
M	molar mass	$\frac{\mathrm{kg}}{\mathrm{mol}}$
n	^{13}CO mole fraction in vapor phase	–
N	^{13}CO mole fraction in liquid phase	–
S	separation factor	–
T	temperature	K
V	vapor molar flow rate per unit area	$\frac{\mathrm{mol}}{\mathrm{m}^2\mathrm{s}}$
x	liquid-phase mole fraction	–
y	vapor-phase mole fraction	–
z	height (position)	m
Z	total height of the column	m
	Greek symbols	
α	relative volatility	–
δ	film thickness	m
ε	enrichment factor	–
θ	number of trays	–
κ	K-value (i.e. vapor-liquid distribution ratio)	–
ρ	density	$\frac{\mathrm{kg}}{\mathrm{m}^3}$
σ	specific interfacial area	$\frac{\mathrm{m}^2}{\mathrm{m}^3}$
τ	molar transfer rate per unit volume	$\frac{\mathrm{mol}}{\mathrm{m}^3\mathrm{s}}$
χ	mole fraction	–
Ψ	product flow rate	$\frac{\mathrm{mol}}{\mathrm{m}^2\mathrm{s}}$
	Superscript	
$*$	hypothetical	–
0	pure component	–
13	atomic number	–
	Subscript	
0	natural abundance	–
^{13}CO	isotopic species	–
c	column	–
H	is referring to H	–
i	index	–
(I)	interface	–
l	liquid	–
L	is referring to L	–
τ	is referring to τ	–
v	vapor	–
V	is referring to V	–

Table 1: Nomenclature

chemical mechanisms, various biological experiments, and medical investigations. Particularly, the interest in the ^{13}C isotope has increased lately due to its applications in organic chemistry, oceanic and atmospheric studies, and medical diagnosis based on breath CO_2 tests ($^{13}C/^{12}C$ ratio), which avoids in this way the common invasive procedures [4, 5].

The isotope separation techniques are based on the isotope effects of different isotopic compounds that arise from the differences in the nuclear properties of the isotopes [6]. Some practical methods are chemical exchange processes, diffusion-based separation, laser separation, chromatography methods, and distillation [7, 8, 9]. The isotope separation technique depends on the properties of the element or the chemical compound involved, the cost of the process, and on the various applications that make use of different concentrations. Due to the relative large mass difference between the different isotopes of light elements like boron, carbon, nitrogen, or oxygen a practical method of isotope separation for these elements is distillation, which is based on the vapor pressure isotope effect [9, 10].

Urey showed in [11] that the isotopic substances differ not only in the physical and chemical properties related directly to mass but in their thermodynamical properties as well. Bigeleisen provides in [12] a method of calculation of the equilibrium constant for the isotopic exchange reactions through methods of statistical mechanics. A general and insightful review on both experimental and theoretical work on the isotope effects with emphasis on the vapor pressure isotope effect is provided by Jancso and Van Hook in [13]. The general theory of multistage isotope separation processes was developed by Cohen [14], treating issues like hold-up, enrichment, and equilibrium time for both ideal and real cascades. The evaporative, concurrent, and countercurrent centrifuges are treated. Cohen also briefly discussed the behavior of liquid-gas countercurrent chemical exchange towers, emphasizing that the theory is essentially the same for all of the isotope separation processes. London [9] also provides an insightful study on isotope separation for reversible and irreversible processes. A chapter in his work is dedicated to the isotope separation by distillation where he briefly presents the production of ^{13}C by the distillation of carbon monoxide. Andreev et al. [15] treat in a descriptive way the methods used in the separation in two-phase systems of hydrogen, carbon, nitrogen, and oxygen, providing also a review based on the characteristics of different ^{13}C cryogenic rectification plants in a chronological order. McInteer presents in [16] design issues of a ^{13}C cryogenic distillation plant by referring to the high-performance plant developed at Los Alamos National Laboratory in the USA. In [17] Li et al. treat the possibility of using advanced structured packing instead of common random packing used in ^{13}C separation from both productivity and reduced consumption points of view while Dulf et al. [18] present a monitoring and control system of a ^{13}C enrichment plant. Mass transfer in fluid systems and the separation processes have been studied extensively, e.g. Cussler and King [19, 20] are excellent references, while in the field of dynamics, operation, and control of distillation columns Skogestad et al. give a comprehensive and insightful exposition in [21, 22, 23, 24]. Regarding modeling of distributed parameter systems we mention [25, 26, 27]. In the field of partial differential equations we acknowledge the work of Debnath [28], while in the numerical analysis field [29, 30, 31] represent standard works.

It is well known that an insightful mathematical description of physical phenomena that occur in various systems is often a requirement for systems analysis, simulation, control design, and optimization [27, 25]. Like most physical, chemical, or biological processes, isotope separation processes have a coupled time-space nature, where the input, output, and parameters can vary both in time and space. Thus, they belong to the class of distributed parameter systems [25].

The objective of this paper is to provide a structured and comprehensive modeling approach followed by the simulation of a ^{13}C isotope separation plant that makes use of the distillation of

carbon monoxide and hence, to provide a basis for future studies in modeling and process control. The main contributions of this study consist in the intelligible first-principles knowledge modeling of the ^{13}C isotope separation process and the assessment of a full nonlinear model and two additional approximation models by numerical simulation. To the authors' best knowledge we are the first to treat these issues for a ^{13}C cryogenic distillation plant.

2. Distillation and the interphase mass transfer

Distillation processes are based on the *relative volatility* notion, which is a comparative measure of the vapor pressure of the components within a mixture. In most of the cases, distillation is carried out in a *tray* column or in a *packed* column [32, 33]. Tray columns are preferred for high ratios of liquid flow rate to vapor flow rate. Packed columns are a practical solution in several situations like low pressure drop separation, handling of corrosive chemicals, or in the case of small column diameter [20, 34]. Since the separation process considered in this paper takes place in a packed tower, packed distillation columns will be referred to in the following.

In this section we will briefly review some distillation and mass transfer-related topics relevant for this study:

- equilibrium stage concept
- vapor-liquid equilibrium
- packed distillation columns
- mass transfer

We refer to the standard works in the field [20, 19, 22, 35] for additional information.

2.1. Equilibrium stage concept

The equilibrium stage (i.e. the theoretical tray) concept is a core concept in distillation processes. It is used for modeling and studying steady-state behavior, for both tray and packed distillation columns.

The equilibrium stage approach states that the vapor and the liquid streams, with the compositions x_{equil} and y_{equil}, leaving the stage are in equilibrium. At equilibrium, even if from a microscopic point of view, temperature, pressure, or composition continue to vary, for a macroscopic observer there are no further changes in these variables [20, 22].

The equilibrium compositions x_{equil} and y_{equil} are mathematically related, as will be shown next.

2.2. Vapor-liquid equilibrium

The vapor-liquid equilibrium relates the composition of the components of a liquid mixture and its vapor at equilibrium. If the mixture is ideal, then the vapor-liquid equilibrium relationship can be derived from Raoult's and Dalton's Laws, which allow the formulation of the K value (vapor-liquid distribution ratio) of a component i [20, 22]:

$$\kappa_i = \frac{y_i}{x_i} = \frac{p_i^0}{P} \tag{1}$$

where y_i and x_i are the vapor and the liquid mole fractions of the component i, p_i^0 is the vapor pressure of the pure component, while P is the total pressure exerted by the gaseous mixture.

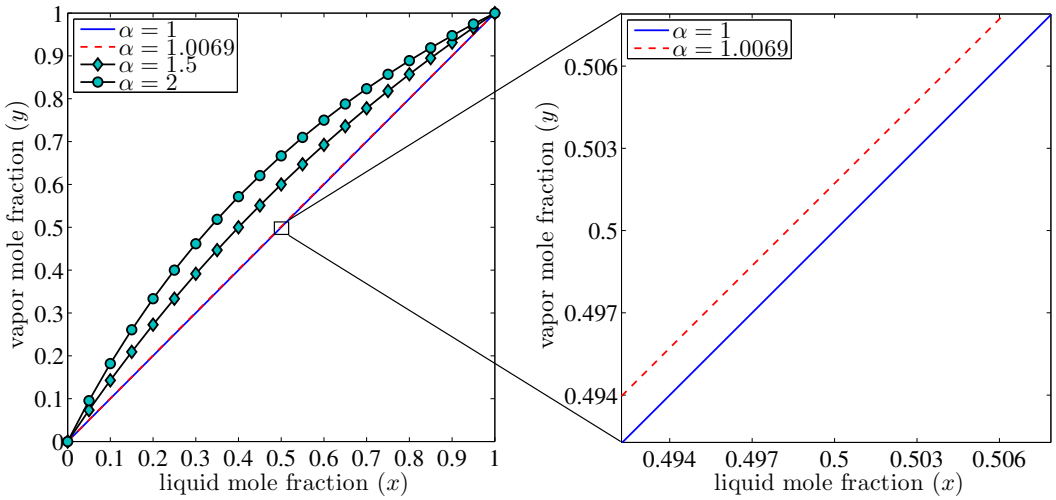

Figure 1: Vapor liquid equilibrium for a binary mixture with respect to different values of α

The relative volatility (α) between the components i and j of a mixture is defined as:

$$\alpha_{ij} = \frac{\kappa_i}{\kappa_j} = \frac{\frac{y_i}{x_i}}{\frac{y_j}{x_j}} = \frac{p_i^0}{p_j^0} \tag{2}$$

where the more volatile component, by convention, is i (so in principle $\alpha_{ij} > 1$).

If the mixture is binary, and y and x refer to the light component, while $1 - y$ and $1 - x$ refer to the heavy component, then the vapor-liquid equilibrium relationship becomes:

$$\alpha = \frac{\frac{y}{x}}{\frac{1-y}{1-x}} = \frac{\frac{y}{1-y}}{\frac{x}{1-x}} \tag{3}$$

or, in a more common form:

$$y = \frac{\alpha x}{1 + (\alpha - 1)x} \tag{4}$$

Figure 1 shows the nonlinear equilibrium curve for a binary mixture with respect to different values of α including the relative volatility in the case of ^{13}C the isotope separation by the distillation of carbon monoxide.

2.3. Packed distillation columns

The role of the packing in a packed distillation column is to ensure an increased contact surface between the vapor and liquid phase and thus, to facilitate the mass transfer. Also the packing must be able to allow pressure drop for the vapor phase and at the same time an easy liquid drainage [35, 34]. For various distillation requirements different types of packing are used. In general, high free spaces and a high surface area improve the efficiency of the packing [33].

In a packed column, the packing bed can be divided into a number of hypothetical zones that act like equilibrium stages. These equilibrium stages are often referred to as theoretical plates [35, 20].

The packing height that accomplish the same separation as an equilibrium stage is referred to as the *height equivalent to a theoretical plate* or HETP and it is a qualitative measure of the packing used.

If the column has θ trays (theoretical or physical), at total reflux with constant relative volatility, Fenske's formula for the overall separation factor applies [22, 36]:

$$S = \frac{\left(\frac{x_{\text{lgt}}}{x_{\text{hvy}}}\right)_{\text{T}}}{\left(\frac{x_{\text{lgt}}}{x_{\text{hvy}}}\right)_{\text{B}}} = \alpha^{\theta} \tag{5}$$

where x_{lgt} and x_{hvy} stand for the light and the heavy component liquid mole fraction while T and B stand for the top of the column respectively the bottom of the column[1]. Since the number of trays is related to the height of the column (Z_{c}) by:

$$\theta = \frac{Z_{\text{c}}}{h_{\text{HETP}}} \tag{6}$$

where h_{HETP} is the value of the HETP, the height equivalent to a theoretical plate is determined by:

$$h_{\text{HETP}} = \frac{Z_{\text{c}}}{\theta} = \frac{Z_{\text{c}} \ln(\alpha)}{\ln(S)} \tag{7}$$

Steady-state behavior of packed columns can be modeled using a staged equilibrium model, this model being used in the column design, but with respect to the dynamics of a packed column, a more appropriate model is based on the mass transfer between the phases [35, 34, 22].

2.4. Interphase mass transfer

Prior to the equilibrium state, considered previously, the vapor and the liquid phase are transferring mass from one to another, with a rate that can be expressed as [34]:

$$\text{mass transfer rate} = k \times (\text{area}) \times (\text{driving force}) \tag{8}$$

where k is called a *mass transfer coefficient* and it is a diffusion rate constant that includes the effect of diffusivity and the flow conditions, the (area) represents the effective mass transfer area, and the (driving force) is the actual cause due to which the mass transfer occurs. Since the driving force can be expressed in terms of concentrations, partial pressure, mole fractions, or molarity, the mass transfer coefficient can also be defined in various ways [20, 19].

There are several theories for describing the mass transfer process [37, 38] among which the two-film theory, the penetration model, the film penetration model, the surface renewal damped eddy diffusion model, or the turbulent diffusion model. Since the two-film theory is widely used, especially for the physical insight it provides into mass transfer and its mathematically simplicity [19], we will adopt this approach.

---

[1] When the product is the heavy component, the separation is given by $S = \frac{\left(\frac{x_{\text{hvy}}}{x_{\text{lgt}}}\right)_{\text{B}}}{\left(\frac{x_{\text{hvy}}}{x_{\text{lgt}}}\right)_{\text{T}}}$.

According to the two-film theory, at any location of the mass transfer equipment, the two-phases compositions are assumed to be constant, except in the liquid and vapor films that exist at the interface. In these stagnant or laminar-flow films, the mass transfer occurs between phases. In addition, at the interface, there is no resistance to mass transfer, the thermodynamical equilibrium being reached almost immediately for a gas and a liquid brought into contact. Thus, the interface compositions are in equilibrium [20, 38].

Diffusion transfer of a component in a binary mixture occurs from one phase to another in the direction of decreasing concentration of that component in both phases adjacent to the interface [20]. For a compound A that is diffusing from vapor to liquid, the vapor bulk mole fraction (y_{A}) will be higher than the interface vapor composition $\left(y_{\mathrm{A(I)}}\right)$, while the liquid interface mole fraction $\left(x_{\mathrm{A(I)}}\right)$ will be higher than the liquid bulk composition (x_{A}).

In steady state, the mass flux of substance A (ϕ_{A}) is constant across the interface and it is given in terms of mole fractions by [39, 34]:

$$\phi_{\mathrm{A}} = k_{\mathrm{v}}\left(y_{\mathrm{A}} - y_{\mathrm{A(I)}}\right) \tag{9}$$

for the vapor phase, and

$$\phi_{\mathrm{A}} = k_{\mathrm{l}}\left(x_{\mathrm{A(I)}} - x_{\mathrm{A}}\right) \tag{10}$$

for the liquid phase, where k_{v} and k_{l} are the *individual*-phase mass transfer coefficients related to physical properties such as hydrodynamic conditions and diffusivity.

The mass transfer rate in terms of the *overall* mass transfer coefficients is given by [20]:

$$\phi_{\mathrm{A}} = K_{\mathrm{v}}(y_{\mathrm{A}} - y^{*}_{\mathrm{A}}) \tag{11}$$

for the vapor phase, and

$$\phi_{\mathrm{A}} = K_{\mathrm{l}}(x^{*}_{\mathrm{A}} - x_{\mathrm{A}}) \tag{12}$$

for the liquid phase, where K_{v} and K_{l} are the overall vapor and liquid-side mass transfer coefficients, while y^{*}_{A} and x^{*}_{A} are the hypothetical vapor and liquid mole fractions that would be in equilibrium with the bulk of the liquid (x_{A}) and the bulk of the vapor (y_{A}).

The vapor and the liquid-side overall mass transfer coefficients (K_{v}, K_{l}) are related to the individual vapor and liquid-phase mass transfer coefficients (k_{v}, k_{l}) by [20, 34]:

$$\frac{1}{K_{\mathrm{v}}} = \frac{1}{k_{\mathrm{v}}} + \frac{m'}{k_{\mathrm{l}}} \tag{13}$$

$$\frac{1}{K_{\mathrm{l}}} = \frac{1}{k_{\mathrm{l}}} + \frac{1}{m'' k_{\mathrm{v}}} \tag{14}$$

where $m' = \frac{y_{\mathrm{A(I)}} - y^{*}_{\mathrm{A}}}{x_{\mathrm{A(I)}} - x_{\mathrm{A}}}$ and $m'' = \frac{y_{\mathrm{A}} - y_{\mathrm{A(I)}}}{x^{*}_{\mathrm{A}} - x_{\mathrm{A(I)}}}$.

3. Isotope separation by cryogenic distillation and the pilot-scale experimental plant

3.1. Isotope separation by cryogenic distillation

Cryogenic distillation is similar to ordinary distillation except that it is used to separate components of a *gaseous mixture* (in standard conditions) [40]. Hence, it is necessary for the process to take place at low temperatures according to the boiling points of the components.

Property	*Symbol*	*Unit*	*Value*
Critical temperature	T_{cr}	K	132.9
Normal boiling point	T_{b}	K	81.6
Normal melting point	T_{m}	K	68.15
Liquid phase density	$\rho_{\mathrm{CO,l}}$	$\frac{\mathrm{kg}}{\mathrm{m}^3}$	788.6
Vapor phase density	$\rho_{\mathrm{CO,v}}$	$\frac{\mathrm{kg}}{\mathrm{m}^3}$	4.355
Enthalpy of vaporization	ΔH_{vap}	$\frac{\mathrm{kJ}}{\mathrm{kg}}$	214.85

Table 2: Carbon monoxide properties used in modeling of the ^{13}C isotope separation process by distillation [41]

In the case of separation of carbon isotopes, it has been shown that the isotope effect based on the pressure difference of saturated vapors of carbon-containing molecules is the highest in the case of carbon monoxide (CO) and methane (CH_4) [13, 15]. Therefore, these substances are preferred as raw material in ^{13}C distillation-based separation.

Since this paper treats the modeling and simulation of a ^{13}C separation plant that makes use of the distillation of carbon monoxide, we have summarized some of the relevant carbon monoxide properties in Table 2. Due to the fact that carbon has two stable isotopes (^{12}C and ^{13}C) and oxygen has three stable isotopes (^{16}O, ^{17}O, and ^{18}O), in the process of cryogenic distillation of carbon monoxide, six molecular species are involved, as can be seen in Table 3. Considering the low natural abundances of ^{17}O and ^{18}O, a reasonable assumption is to relate the carbon monoxide to a binary mixture form of ^{12}C^{16}O and ^{13}C^{16}O. Hence, referring to (2) and considering that ^{13}CO (the less volatile component) is the product, the separation factor is expressed as follows[2] :

$$\alpha = \frac{p^0_{^{12}\mathrm{CO}}}{p^0_{^{13}\mathrm{CO}}} = \frac{\frac{N}{1-N}}{\frac{n}{1-n}} \tag{15}$$

where N and n refer to the ^{13}CO mole fraction in the liquid respectively vapor phase; so $1-N$ and $1-n$ represent the ^{12}CO mole fraction in the liquid respectively vapor phase.

There are several methods for determining α values for the $^{12}\mathrm{CO} - {}^{13}\mathrm{CO}$ mixture like Rayleigh distillation or differential pressure techniques [13]. Analytically, the *enrichment factor* (ε) over the temperature range of $68.2\,\mathrm{K} - 81.2\,\mathrm{K}$ (the common interval within which the CO distillation takes place), is described by Johns [42]:

$$\varepsilon = \frac{78.2}{T^2} - \frac{0.394}{T} \tag{16}$$

where $\varepsilon = \alpha - 1$ and T is the temperature at which the process occurs. An accepted value for α at the normal boiling point (T_{b}) of CO is $\alpha = 1.0069$, or in other words, ^{12}CO has about a 0.69% higher vapor pressure than ^{13}CO [15].

3.2. The pilot-scale experimental plant

The experimental pilot-scale plant that was developed at the National Institute for Research and Development of Isotopic and Molecular Technologies in Cluj-Napoca, Romania is shown in Figure 2.

[2]For brevity the atomic number of the oxygen is omitted.

	Atomic mass/Molecular mass (u)	*Natural Abundance* (%)
Carbon		
^{12}C	12	98.89
^{13}C	13	1.11
Oxygen		
^{16}O	16	99.76
^{17}O	17	0.04
^{18}O	18	0.20
Carbon monoxide		
$^{12}C^{16}O$	28	98.6527
$^{12}C^{17}O$	29	0.0396
$^{12}C^{18}O$	30	0.1978
$^{13}C^{16}O$	29	1.1073
$^{13}C^{17}O$	30	0.0004
$^{13}C^{18}O$	31	0.0022

Table 3: Isotopic forms of carbon, oxygen, and carbon monoxide and their abundances

The distillation column is configurable in several ways, however, in this paper we will consider a configuration that consists of one column of 7000 mm in height and an inner diameter of 16 mm which operates in total-reflux regime at a pressure of approximately 0.8 atm. The column is packed with Heli-Pak stainless steel wire of $1.8 \times 1.8 \times 0.2$ mm, which has an HETP value of approximately 20 mm.

Highly purified carbon monoxide is fed up the column, and the extracted waste gas (^{12}CO enriched) is taken out from the top of the column, while the ^{13}C enriched product (^{13}CO enriched) is withdrawn at the base of the column. The vapor stream is ensured by a variable heating resistance (up to 150 W) and the total condenser provides the reflux. The condenser uses liquid nitrogen as cooling agent (N_2 has a boiling point of T_b=77.3 K), and is provided with surface-increasing elements for a better efficiency in the heat exchange between CO vapors and the liquid nitrogen. The cryogenic distillation plant is insulated by a multilayered vacuum jacket. The pressure in the jacket was $8 \cdot 10^{(-5)}$ torr.

4. Mathematical modeling

The isotope exchange process involving the redistribution of ^{12}C and ^{13}C between the liquid and the vapor phase of the same isotopic compound in physical equilibrium is expressed by [1]:

$$^{12}CO_{(\text{liquid})} + {}^{13}CO_{(\text{vapor})} \rightleftarrows {}^{13}CO_{(\text{liquid})} + {}^{12}CO_{(\text{vapor})} \tag{17}$$

In order to derive the mathematical description of the concerned isotope separation process we will proceed as follows. Firstly, based on the two-film theory of the interphase mass transfer, we will derive the rate of transfer of the ^{13}C isotope from the vapor phase to the liquid phase followed by the deriving of the physical description of the overall mass transfer coefficient. From the mass balance relations we will derive the system of equations that governs the evolution of ^{13}C isotope

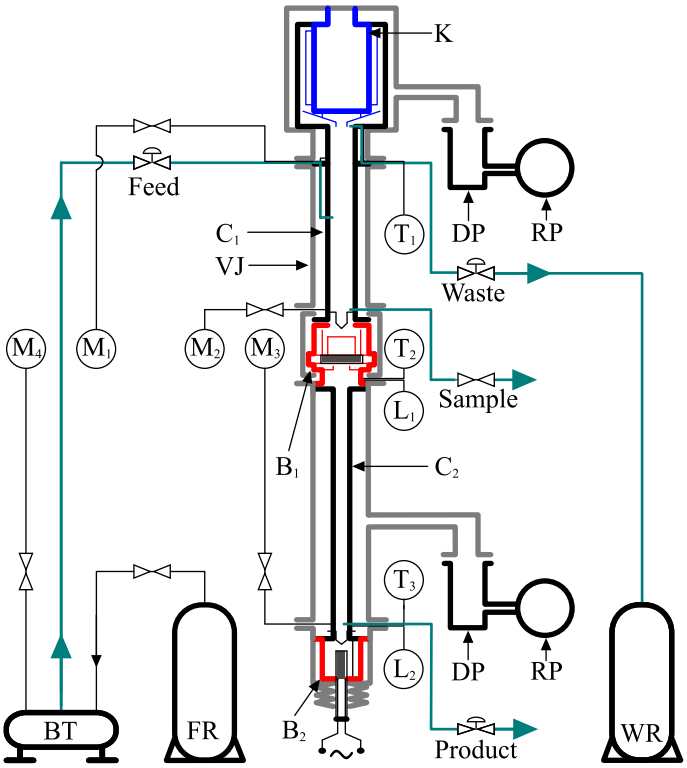

Figure 2: Experimental pilot-scale cryogenic distillation plant with condenser K, primary column C_1, final column C_2, reboilers B_1-B_2, vacuum jacket VJ, rough pump RP, diffusion pump DP, temperature sensors T_1-T_3, manometers M_1-M_4, level sensors L_1-L_2, feed reservoir FR, buffer tank BT, waste reservoir WR

with respect to time and height in both the liquid and the vapor phase. Next, we will determine the volumetric overall mass transfer coefficient as a function of the plant parameters. Finally, we will solve the system of equations that describe the evolution of ^{13}C isotope with respect to ^{13}CO liquid mole fraction.

4.1. The isotopic mass transfer rate

Since the interfacial mass transfer is proportional to the specific interfacial area, an insightful description of the mass transfer rate is the *mass transfer rate per unit of volume of transfer device* [35, 43].

In the case of our isotope separation process, the specific interfacial area is a property related to the surface area and to the volume of the column packing. Referring to the general form mass transfer equation (8), and dividing both sides of the relation by the (volume), we obtain:

$$\left(\frac{\text{mass transfer rate}}{\text{volume}}\right) = k \times \sigma \times (\text{driving force}) \tag{18}$$

where σ is the *specific interfacial area*.

If $\tau = \frac{\text{mass transfer rate}}{\text{volume}}$ is the rate of transfer of the desired isotope to the enriched phase across the interface per unit of volume [14], then, in steady state, the isotopic mass flux in terms of mole fractions is given by:

$$\frac{\tau}{\sigma} = k_{\mathrm{v}}\big(n - n_{(\mathrm{I})}\big) \tag{19}$$

$$\frac{\tau}{\sigma} = k_{\mathrm{l}}\big(N_{(\mathrm{I})} - N\big) \tag{20}$$

where n and N represent ^{13}CO mole fractions in the bulk of vapor respectively in the bulk of liquid, while $n_{(\mathrm{I})}$ and $N_{(\mathrm{I})}$ are the vapor and liquid interface mole fractions of ^{13}CO.

Since according to the two-film theory, $N_{(\mathrm{I})}$ and $n_{(\mathrm{I})}$ are in equilibrium, then, with reference to (15):

$$n_{(\mathrm{I})} = \frac{N_{(\mathrm{I})}}{\alpha - (\alpha - 1)N_{(\mathrm{I})}} \tag{21}$$

Hence,

$$N_{(\mathrm{I})} - n_{(\mathrm{I})} = n_{(\mathrm{I})}(\alpha - 1)\big(1 - N_{(\mathrm{I})}\big) \tag{22}$$

By referring to (19), (20), and(22) an expression for τ follows:

$$\tau = K\big[(n - N) + n_{(\mathrm{I})}(\alpha - 1)\big(1 - N_{(\mathrm{I})}\big)\big] \tag{23}$$

where

$$\frac{1}{K} = \frac{1}{k_{\mathrm{v}}\sigma} + \frac{1}{k_{\mathrm{l}}\sigma} \tag{24}$$

Here, K can be identified with the *volumetric* overall mass transfer coefficient [35].

Due to the fact that in the case of isotope separation, the interfacial concentrations have values very close to the associated bulk concentrations [14] and thus $N_{(\mathrm{I})} \approx N$, $n_{(\mathrm{I})} \approx n$, the relation (23) can be rewritten in the following form:

$$\tau = -K\big[(N - n) - n(\alpha - 1)(1 - N)\big] \tag{25}$$

For deriving the physical description of the volumetric overall mass transfer coefficient, we refer to Fick's first law of diffusion [20], which states that the mass flux occurs from high-concentration regions to low-concentration regions, and that it is proportional to the concentration gradient by a diffusion coefficient:

$$J_{\mathrm{A}} = -D\nabla c_{\mathrm{A}} \tag{26}$$

where J_{A} is the molar flux, D is the molecular diffusivity, and ∇c_{A} is the gradient of molar concentration of component A. In one spatial dimension[3] (26) becomes:

$$J_{\mathrm{A}} = -D\frac{\partial c_{\mathrm{A}}}{\partial z} \tag{27}$$

where z represents the position.

[3]Since the mass transfer device in the case of isotope separation by cryogenic distillation is usually a very long column with a small diameter, a good approximation arises by considering only the longitudinal effects (in our case the column is 7000 mm in length and 16 mm in diameter).

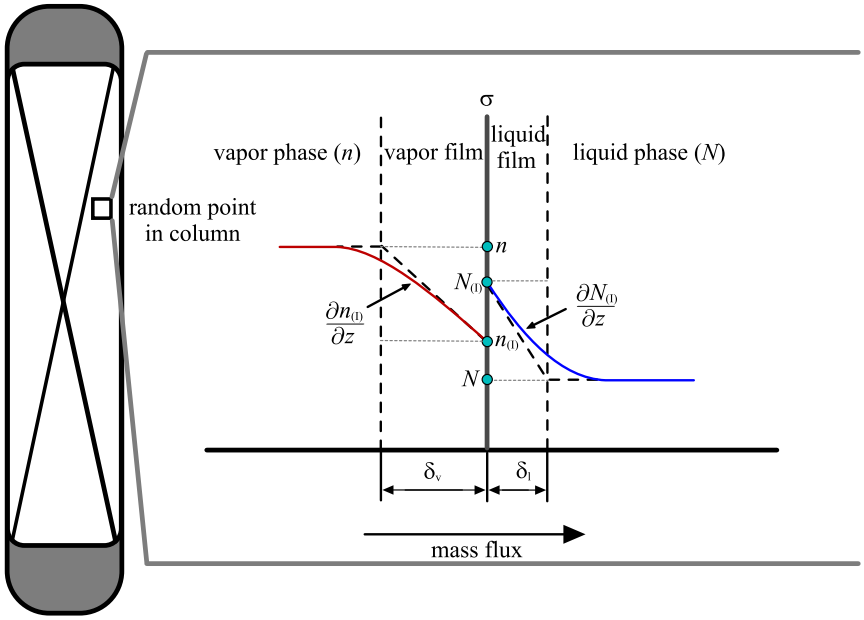

Figure 3: ^{13}C isotope interphase mass transfer according to the two-film theory

Since the molar concentration of a component i (c_i) is related to its mole fraction (χ_i) by:

$$c_i = \chi_i \frac{\rho}{\overline{M}} \tag{28}$$

where ρ is the density of the solution and $\overline{M}$ represents the average molar mass of the solution, then, in steady state, the isotopic molar flux is:

$$\begin{aligned} \frac{\tau}{\sigma} &= -D_{\mathrm{v}} \frac{\rho_{\mathrm{CO,v}}}{\overline{M}_{\mathrm{CO}}} \frac{\partial n_{(\mathrm{I})}}{\partial z} \\ &= -D_{\mathrm{l}} \frac{\rho_{\mathrm{CO,l}}}{\overline{M}_{\mathrm{CO}}} \frac{\partial N_{(\mathrm{I})}}{\partial z} \end{aligned} \tag{29}$$

where D_{v} and D_{l} stand for diffusion coefficients in the vapor and the liquid phase, $\rho_{\mathrm{CO,v}}$ and $\rho_{\mathrm{CO,l}}$ are the vapor and the liquid phase carbon monoxide density, while $\overline{M}_{\mathrm{CO}}$ is the average carbon monoxide molar mass. Referring to the Figure 3, where the interphase mass transfer of ^{13}C isotope according to the two-film theory is represented, we obtain the linearized differential coefficients:

$$\begin{aligned} \frac{\partial n_{(\mathrm{I})}}{\partial z} &\approx \frac{n_{(\mathrm{I})} - n}{\delta_{\mathrm{v}}} \\ \frac{\partial N_{(\mathrm{I})}}{\partial z} &\approx \frac{N - N_{(\mathrm{I})}}{\delta_{\mathrm{l}}} \end{aligned} \tag{30}$$

where δ_{v} and δ_{l} are the vapor and liquid film thicknesses.

From (29) and (30) the physical description of the volumetric overall mass transfer coefficient follows:

$$\frac{1}{K} = \frac{1}{\sigma}\frac{\overline{M}_{\mathrm{CO}}\delta_{\mathrm{v}}}{D_{\mathrm{v}}\rho_{\mathrm{CO,v}}} + \frac{1}{\sigma}\frac{\overline{M}_{\mathrm{CO}}\delta_{\mathrm{l}}}{D_{\mathrm{l}}\rho_{\mathrm{CO,l}}} \tag{31}$$

4.2. The isotopic mass balance equations

For determining the isotopic mass balance equations we will consider a column element as shown in Figure 4(a). The column element, of height dz and diameter d, lies between heights z and $z+dz$. In the figure, L and V are the liquid and vapor molar flow rates of the ^{12}CO and ^{13}CO mixture per cross section area of the column (A_{c}), while $L_{^{13}\mathrm{CO}}$ and $V_{^{13}\mathrm{CO}}$ denote the ^{13}CO liquid and vapor molar flow rates. At height z, the liquid molar flow rate $L_{^{13}\mathrm{CO}}(z,t)$ is entering the column element, while the vapor molar flow rate $V_{^{13}\mathrm{CO}}(z,t)$ is leaving the column element. At height $z+dz$, the liquid and the vapor molar flow rates are leaving, respectively entering the column element. Since the heavy isotope is accumulating in the liquid phase the height will be measured by convention in the liquid flow direction.

If $\nu_{L_{^{13}\mathrm{CO}}}(z,t)$ is the number of ^{13}CO moles in the liquid phase that are entering the column element between t and $t+dt$, then the ^{13}CO liquid molar flow rate at height z per cross section area of the column is defined by:

$$L_{^{13}\mathrm{CO}}(z,t) = \frac{\nu_{L_{^{13}\mathrm{CO}}}(z,t)}{A_{\mathrm{c}}dt} \tag{32}$$

Analogously, the ^{13}CO vapor molar flow rate at height z is defined by:

$$V_{^{13}\mathrm{CO}}(z,t) = \frac{\nu_{V_{^{13}\mathrm{CO}}}(z,t)}{A_{\mathrm{c}}dt} \tag{33}$$

Recalling the notions presented in Section 4.1, the number of moles transferred from the vapor phase to the liquid phase (ν_τ), in the volume $dv = A_{\mathrm{c}}dz$, in the time between t and $t+dt$, is defined by:

$$\nu_\tau = \tau dv dt \tag{34}$$

At time t in the column element there is a certain number of ^{13}CO moles referred to as ^{13}CO *hold-up*.

Figure 4(b) emphasizes the time evolution of the ^{13}CO hold-up per volume element in the liquid ($H_{^{13}\mathrm{CO,l}}$) and in the vapor phase ($H_{^{13}\mathrm{CO,v}}$). The liquid ^{13}CO hold-up in the column element, at time t is defined by:

$$H_{^{13}\mathrm{CO,l}}(z,t) = \frac{\nu_{H_{^{13}\mathrm{CO,l}}}(z,t)}{dv} \tag{35}$$

where $\nu_{H_{^{13}\mathrm{CO,l}}}(z,t)$ is the number of ^{13}CO moles in the column element in the liquid phase at time t. Analogously, the vapor ^{13}CO hold-up per column element is defined by:

$$H_{^{13}\mathrm{CO,v}}(z,t) = \frac{\nu_{H_{^{13}\mathrm{CO,v}}}(z,t)}{dv} \tag{36}$$

Since no chemical reaction takes place, the isotopic mass balance for the liquid phase, in the column element, in the time span between t and $t+dt$, is described in terms of number of moles by:

$$\underbrace{(\nu_{L_{^{13}\mathrm{CO}}}(z,t)+\nu_\tau)}_{\text{mass in}} - \underbrace{\nu_{L_{^{13}\mathrm{CO}}}(z+dz,t)}_{\text{mass out}} = \underbrace{\nu_{H_{^{13}\mathrm{CO,l}}}(z,t+dt) - \nu_{H_{^{13}\mathrm{CO,l}}}(z,t)}_{\text{accumulation}} \tag{37}$$

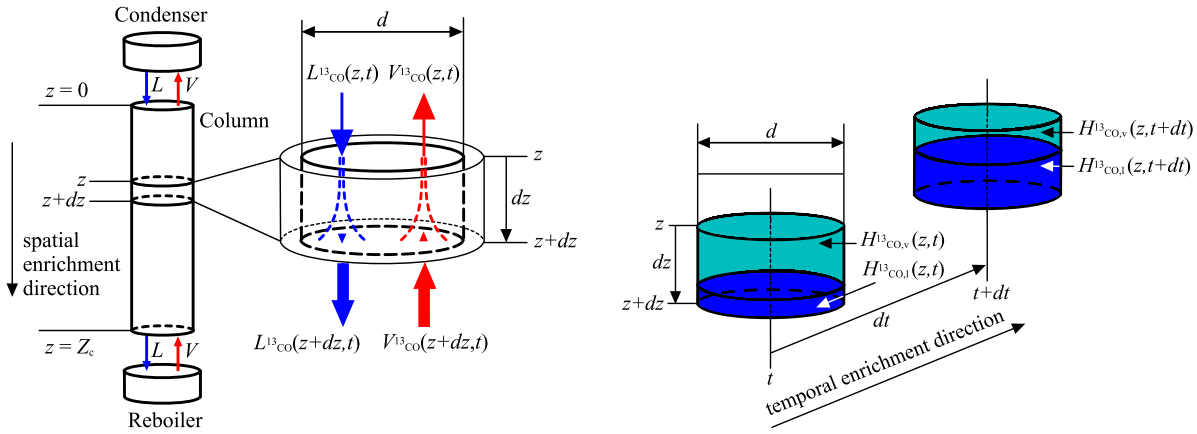

(a) Isotope enrichment with respect to height

(b) Isotope enrichment with respect to time

Figure 4: The column element and the ^{13}C isotope enrichment with respect to height and time

For the vapor phase, a similar relation holds:

$$\nu_{V_{^{13}\mathrm{CO}}}(z+dz,t) - (\nu_{V_{^{13}\mathrm{CO}}}(z,t) + \nu_\tau) = \nu_{H_{^{13}\mathrm{CO,v}}}(z,t+dt) - \nu_{H_{^{13}\mathrm{CO,v}}}(z,t) \tag{38}$$

By referring to (32), (34), and (35), (37) becomes:

$$\begin{aligned}(L_{^{13}\mathrm{CO}}(z,t)A_c dt + \tau dv dt) - L_{^{13}\mathrm{CO}}(z+dz,t)A_c dt = & H_{^{13}\mathrm{CO,l}}(z,t+dt)dv - \\ & - H_{^{13}\mathrm{CO,l}}(z,t)dv\end{aligned} \tag{39}$$

which leads to:

$$\frac{H_{^{13}\mathrm{CO,l}}(z,t+dt) - H_{^{13}\mathrm{CO,l}}(z,t)}{dt} + \frac{L_{^{13}\mathrm{CO}}(z+dz,t) - L_{^{13}\mathrm{CO}}(z,t)}{dz} = \tau \tag{40}$$

Since the rate of change in the number of ^{13}CO moles in the liquid phase that are passing through the column element between the heights z and $z+dz$ is given by:

$$\frac{\partial \nu_{L_{^{13}\mathrm{CO}}}(z,t)}{\partial z} = \frac{\nu_{L_{^{13}\mathrm{CO}}}(z+dz,t) - \nu_{L_{^{13}\mathrm{CO}}}(z,t)}{dz} \tag{41}$$

while the rate of change in the number of ^{13}CO moles that are accumulating in the column element in the liquid phase between the time t and the time $t+dt$ is:

$$\frac{\partial \nu_{H_{^{13}\mathrm{CO,l}}}(z,t)}{\partial t} = \frac{\nu_{H_{^{13}\mathrm{CO,l}}}(z,t+dt) - \nu_{H_{^{13}\mathrm{CO,l}}}(z,t)}{dt} \tag{42}$$

then, in terms of mole fractions, (40) becomes:

$$H_l \frac{\partial N(z,t)}{\partial t} + L \frac{\partial N(z,t)}{\partial z} = \tau \tag{43}$$

where H_{l} is the ^{12}CO and ^{13}CO (i.e. the raw material) hold-up in the liquid phase and L is the liquid molar flow rate per cross section area of the column of the ^{12}CO and ^{13}CO mixture. Analogously, for the vapor phase, the following relation holds:

$$H_{\mathrm{v}}\frac{\partial n(z,t)}{\partial t} - V\frac{\partial n(z,t)}{\partial z} = -\tau \tag{44}$$

The relations (43) and (44) describe the rate of change of the heavy isotope (i.e. the product) in time and height, in the liquid and vapor phase, with respect to associated plant variables, H_{l}, H_{v}, L, V, and τ.

4.3. The volumetric overall mass transfer coefficient

The volumetric overall mass transfer coefficient is related to physical properties like molecular diffusivity and vapor and liquid-phase film thickness, which are very difficult to measure [20, 19]. However, in the following we will estimate the value of the mass transfer coefficient, based on the plant parameters by referring to the isotopic mass balance relations (43), (44) and to the rate of transfer per unit volume defined by (25).

At steady state, (43) and (44) become[4]:

$$L\frac{dN}{dz} = -K\big[(N-n) - n(\alpha-1)(1-N)\big] \tag{45}$$

$$-V\frac{dn}{dz} = K\big[(N-n) - n(\alpha-1)(1-N)\big] \tag{46}$$

When no withdrawal is performed, and thus the liquid is converted entirely into vapor, the column being operated in total-reflux regime, the isotopic mole fractions are equal at the ends of the column, and in addition, the internal streams are equal:

$$\begin{gathered} N(z=Z_{\mathrm{c}}) = n(z=Z_{\mathrm{c}}) \\ L = V \\ N(z=0) = n(z=0) \end{gathered} \tag{47}$$

Therefore, the steady-state relations (45) and (46) are reduced to:

$$L\frac{dN}{dz} = K(\alpha-1)N(1-N) \tag{48}$$

If we denote by λ the term $\frac{K(\alpha-1)}{L}$, it can be easily observed that the relation is similar to the *Verhulst-Pearl logistic equation*, which describes the population growth in an environment with limited resources [44]:

$$\frac{dN}{dz} = \lambda N\left(1 - \frac{N}{\mu}\right) \tag{49}$$

[4]For the sake of brevity we will not explicitly put z as argument for N and n

where λ represents the intrinsic growth rate and μ is the saturation level, with the growth taking place not in time, but in space. Since the growth applies to mole fractions the saturation level is equal to unity. Thus, the solution of (49) is:

$$N(z) = \frac{e^{\lambda z}\gamma}{1 + e^{\lambda z}\gamma} \tag{50}$$

where γ is a constant of integration that can be determined from the initial condition. Therefore, the ^{13}C enrichment in the liquid phase with respect to the height follows:

$$N(z) = \frac{1}{1 + \left(\frac{1-N_0}{N_0}\right) e^{-\frac{K(\alpha-1)z}{L}}} \tag{51}$$

where N_0 stands for natural ^{13}C isotopic abundance.

The overall volumetric mass transfer coefficient K may now be determined from (51), written for the boundary condition ($z = Z_c$), and it is equal to:

$$K = \frac{L}{(\alpha-1)Z_c} \ln\left(\frac{\frac{N(Z_c)}{1-N(Z_c)}}{\frac{N_0}{1-N_0}}\right) \tag{52}$$

4.4. The isotope separation partial differential equations

The system of Partial Differential Equations (PDEs) (43)-(44) can be solved in terms of the ^{13}CO liquid mole fraction (N), by describing the ^{13}CO vapor mole fraction (n) from (25) and (43) as:

$$n = \frac{\frac{H_l}{K}\frac{\partial N}{\partial t} + \frac{L}{K}\frac{\partial N}{\partial z} + N}{1 + (\alpha-1)(1-N)} \tag{53}$$

and computing its partial derivatives with respect to time and height:

$$\frac{\partial n}{\partial t} = \frac{\left(\frac{H_l}{K}\frac{\partial^2 N}{\partial t^2} + \frac{L}{K}\frac{\partial^2 N}{\partial t \partial z} + \frac{\partial N}{\partial t}\right)A + \frac{\partial N}{\partial t}(\alpha-1)B}{A^2} \tag{54}$$

$$\frac{\partial n}{\partial z} = \frac{\left(\frac{H_l}{K}\frac{\partial^2 N}{\partial z \partial t} + \frac{L}{K}\frac{\partial^2 N}{\partial z^2} + \frac{\partial N}{\partial z}\right)A + \frac{\partial N}{\partial z}(\alpha-1)B}{A^2} \tag{55}$$

where $A = \left[1 + (\alpha-1)(1-N)\right]$ and $B = \left(\frac{H_l}{K}\frac{\partial N}{\partial t} + \frac{L}{K}\frac{\partial N}{\partial z} + N\right)$.

From the relations set (43), (44), (53), (54), (55) we obtain the following PDE:

$$\begin{aligned}
&\frac{\partial^2 N}{\partial t^2}\left(\frac{AH_vH_l}{K}\right) + \frac{\partial N}{\partial t}\left[AH_v + BH_v(\alpha-1) + A^2H_l\right] = \\
&= \frac{\partial^2 N}{\partial z \partial t}\left[A\left(\frac{VH_l}{K} - \frac{LH_v}{K}\right)\right] + \frac{\partial^2 N}{\partial z^2}\left(\frac{ALV}{K}\right) + \frac{\partial N}{\partial z}\left[AV + BV(\alpha-1) - A^2L\right]
\end{aligned} \tag{56}$$

where we took into account Young's Theorem on the equality of mixed partial derivatives [45]. In the following, (56) will be referred to as the *full nonlinear* isotope separation PDE model.

However, knowing that the concentration varies very slowly due to the low enrichment factor (i.e. $\varepsilon = \alpha - 1 \approx 0.0069$ [13, 15]) and that the steady-state regime is achieved after several days only, one can neglect the second-order derivative in time, the mixed derivatives, and the terms containing $\frac{\partial N}{\partial t}(\alpha - 1)$ and $\frac{\partial N}{\partial z}(\alpha - 1)B$.

After these simplifications and knowing that the bottom product flow rate in the column (Ψ) is given by $\Psi = L - V$, the following PDE follows:

$$(H_{\mathrm{l}} + H_{\mathrm{v}})\frac{\partial N}{\partial t} = \left(\frac{LV}{K}\right)\frac{\partial^2 N}{\partial z^2} - \frac{\partial N}{\partial z}\big[\Psi + L(\alpha - 1)(1 - N)\big] \tag{57}$$

and it will be referred as the *quasi-linear* isotope separation PDE model.

The general form of (57):

$$c_6\frac{\partial N}{\partial t} = c_5\frac{\partial^2 N}{\partial s^2} - \frac{\partial}{\partial s}\big[\Psi N + c_1 N(1 - N)\big] \tag{58}$$

where c_6, c_5, Ψ, and, c_1 are constants, is referred to in [14] as the *fundamental equation* of isotope separation.

Since the ^{13}CO liquid phase mole fraction $N \ll 1$, (57) may be furthermore simplified to the following form:

$$(H_{\mathrm{l}} + H_{\mathrm{v}})\frac{\partial N}{\partial t} = \left(\frac{LV}{K}\right)\frac{\partial^2 N}{\partial z^2} - \frac{\partial N}{\partial z}\big[\Psi + L(\alpha - 1)\big] \tag{59}$$

which will be referred to as the *linear* isotope separation PDE model.

5. Numerical analysis

Previously we have determined the full nonlinear isotope separation PDE model (56) and based on certain assumptions we have derived two simplified models, a quasi-linear (57) and a linear model (59). In this section we will proceed with numerical analysis issues in order to numerically solve and simulate these models.

For obtaining a *finite-dimensional* system of difference equations or ordinary differential equations to numerically solve a PDE one can consider methods like finite-difference, finite-element, finite-volume, or weighted-residual methods [25, 46, 30]. In the case of a problem with a simple geometry finite-difference and spectral methods are suitable choices [25]. For problems with a complex geometry or complicated boundary conditions one can chose finite-element or finite-volume methods [47, 30].

Since the main advantage of the finite-difference methods is the flexibility in dealing with nonlinear problems and since in addition they are easy to implement [30, 48], we will choose the finite-difference method for analysis of the three models.

As is well known, for a numerical method, *consistency*, *stability*, and *convergence* are the most important aspects [30]. As a reminder, a finite-difference equation is consistent if the truncation error approaches zero (this is usually the case for finite-difference approximations derived from Taylor series), it is stable if the error remains uniformly bounded, and it is convergent if its solution approaches that of the partial differential equation as the grid size approaches zero [30, 48].

Let the ^{13}CO liquid mole fraction function $N(z, t)$ be identified with $u(i, j)$. The two integer indices i and j indicates where the quantity is evaluated and are related to the Cartesian coordinates

as follows:

$$z(i) = z_0 + i\Delta z$$
$$t(j) = t_0 + j\Delta t$$

The grid has a fixed mesh spacing Δz in the z-direction and Δt in the t-direction. Considering the expansions in Taylor series around a point $(z(i), t(j))$ [30], the *forward-difference* approximation for $\frac{\partial N}{\partial z}$ and $\frac{\partial N}{\partial t}$ at the coordinates $(z(i), t(j))$ is:

$$\frac{\partial N}{\partial z} = u_z(i,j) \approx \frac{u(i+1,j) - u(i,j)}{\Delta z} \tag{60}$$

$$\frac{\partial N}{\partial t} = u_t(i,j) \approx \frac{u(i,j+1) - u(i,j)}{\Delta t} \tag{61}$$

where Δz and Δt represent the grid size in the height and in the time dimension.

The *backward-difference* approximation for $\frac{\partial N}{\partial t}$ is given by:

$$\frac{\partial N}{\partial t} = u_t(i,j) \approx \frac{u(i,j) - u(i,j-1)}{\Delta t} \tag{62}$$

The second-order *central* difference for $\frac{\partial^2 N}{\partial z^2}$ and $\frac{\partial^2 N}{\partial t^2}$ are given by:

$$\frac{\partial^2 N}{\partial z^2} = u_{zz}(i,j) \approx \frac{u(i+1,j) - 2u(i,j) + u(i-1,j)}{(\Delta z)^2} \tag{63}$$

$$\frac{\partial^2 N}{\partial t^2} = u_{tt}(i,j) \approx \frac{u(i,j+1) - 2u(i,j) + u(i,j-1)}{(\Delta t)^2} \tag{64}$$

Finally, the mixed derivative $\frac{\partial^2 N}{\partial z \partial t}$ approximation is given by:

$$\frac{\partial^2 N}{\partial z \partial t} = u_{zt}(i,j) \approx \frac{u(i,j) - u(i-1,j) - u(i,j-1) + u(i-1,j-1)}{\Delta z \Delta t} \tag{65}$$

Using (60)−(65) we will numerically solve the PDE models (56), (57), and (59)

The time-space domain of our distributed parameter system is determined by the duration of the total-reflux experiment and by the length of the column. The initial condition is represented by the natural abundance of ^{13}C, while the boundary conditions are determined by the concentration achieved at the top of the column ($z = 0$) respectively at the bottom of the column ($z = Z_c$).

During the total-reflux experiment, samples were collected from both ends of the column every 12 hours (see Figure 5). The plant operated in total-reflux regime for 96 hours and the electrical power that supplied the heating resistance was 30 W. The two curves shown in Figure 5 representing the boundary conditions used in numerical analysis were obtained by the use of a fifth-order polynomial interpolation that fits the data in a least-squares sense.

Since this experiment was conducted in the total-reflux regime, the vapor and liquid internal streams were equal ($L = V$). The vapor internal stream was determined by knowing the electrical power which supplied the heating resistance and the heat transfer through the multilayered vacuum jacket [49], [50] used for insulation.

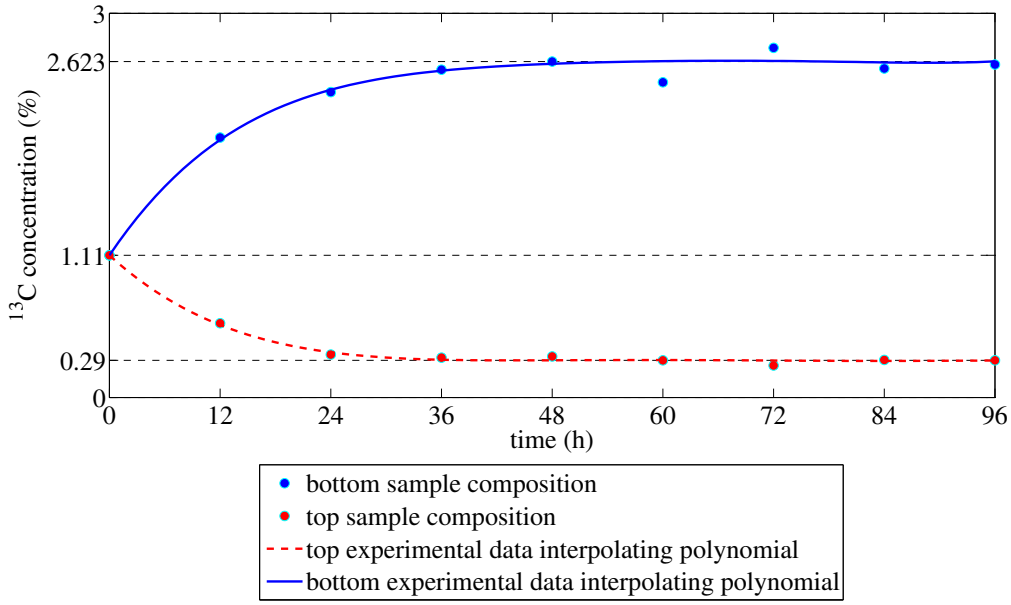

Figure 5: ^{13}C concentrations achieved by the pilot-scale experimental plant

The total hold-up in the column ($H_{\text{tot}} = H_{\text{l}} + H_{\text{v}}$) was determined by measuring the quantity of raw material fed to the column during the operations prior to the beginning of the experiment. The vapor phase hold-up (H_{v}) was determined by measuring the electrical power which supplied the heating resistance and knowing the heat received through the multilayered vacuum jacket used for insulation. Hence, the liquid phase hold-up (H_{l}) was determined by:

$$H_{\text{l}} = H_{\text{tot}} - H_{\text{v}} \tag{66}$$

6. Results and discussion

In the case of linear PDEs, for a well-posed initial-value problem and a consistent finite-difference scheme, the Lax equivalence theorem applies [29], stability being the necessary and sufficient condition for convergence. Therefore, we have used the linear PDE model (59) as reference model for the convergence of the solution. However, for all the schemes used in the simulations, whenever the stability was achieved, the full nonlinear (56) and the quasi-linear model (57) were convergent too. This fact is not surprising at all since the nonlinear terms are close to zero, thus confirming the assumptions made in Section 4.4.

Figures 6(a) and 6(b) show the ^{13}CO mole fraction distribution in the column with respect to both height and time. The isotope distribution was obtained by simulating the full nonlinear model (56) for 50 discretization divisions applied to the space domain (i.e. $\Delta z = \frac{7}{50}$m) and a time step (Δt) equal to 0.5 seconds. In order to compare the isotope separation process models, for the same mesh spacing, we simulated the linear and the quasi-linear models. The simulation time of the

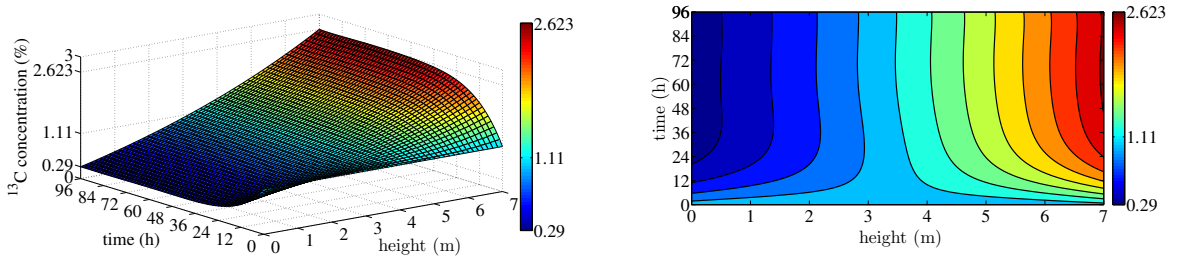

(a) ^{13}C isotope concentration distribution (b) ^{13}C isotope concentration distribution (contour view)

Figure 6: ^{13}C isotope concentration distribution with respect to time and height

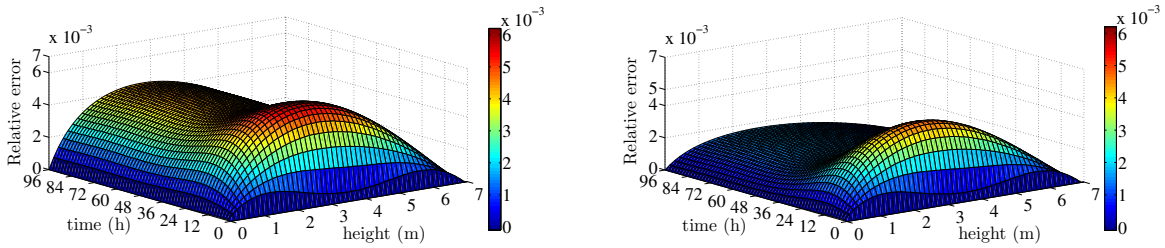

(a) Relative error of the linear model (b) Relative error of the quasi-linear model

Figure 7: Relative errors of the linear and quasi-linear models

linear model was approximately 16.5 seconds, while the simulation time of the quasi-linear model was approximately 17 seconds. The simulation time of the full nonlinear model was 5 minutes and 10 seconds.

Figures 7(a) and 7(b) show the relative errors of the simplified models over the time-space domain. Explicitly, in the case of the linear model, the relative error is:

$$\xi_{\text{linear}}(z,t) = \left| \frac{N_{\text{nonlinear}}(z,t) - N_{\text{linear}}(z,t)}{N_{\text{nonlinear}}(z,t)} \right| \tag{67}$$

The relative error of the quasi-linear model is defined similarly:

$$\xi_{\text{quasi-linear}}(z,t) = \left| \frac{N_{\text{nonlinear}}(z,t) - N_{\text{quasi-linear}}(z,t)}{N_{\text{nonlinear}}(z,t)} \right| \tag{68}$$

The simulations were repeated for various schemes, using from 65 to 35 space discretization divisions and different time steps with values between 0.54 seconds to 36 seconds. If the numerical calculation using the scheme was stable, the results of the simulations performed were very similar with those presented in Figures 6(a) and 6(b) with no visible differences. In each case, the maximum and the average relative errors $\big(\max\big(\xi(z,t)\big)$ and $\overline{\xi(z,t)}\big)$ for the two approximation models over

the time-space interval are bounded by very narrow bounds:

$$\begin{aligned}
\max\big(\xi_{\text{linear}}(z,t)\big) &\in \big[0.00603,\ 0.00633\big] \\
\max\big(\xi_{\text{quasi-linear}}(z,t)\big) &\in \big[0.00508,\ 0.00528\big] \\
\overline{\xi_{\text{linear}}(z,t)} &\in \big[0.00291,\ 0.00327\big] \\
\overline{\xi_{\text{quasi-linear}}(z,t)} &\in \big[0.00145,\ 0.00179\big]
\end{aligned}$$

The advantage of the full nonlinear model is that it can be applied in a variety of isotope separation processes, since no simplifying assumptions were made. The drawback of the full nonlinear model is its high complexity, which also leads to a long simulation time. However, in most of the isotope separation processes, the concentration varies very slowly due to the low enrichment factor, leading to a simpler model, the quasi-linear model. When the isotope concentration achieved during the separation process is low, a valid modeling approach is the linear model, which is also the simplest and fastest model.

The maximum relative error of $\pm 0.6\%$ and the average relative error of $\pm 0.3\%$ in the case of the linear model, respectively $\pm 0.5\%$ and $\pm 0.15\%$ in the case of the quasi-linear model, show that the finite difference schemes are consistent and convergent.

7. Conclusions

With the increasing complexity of the processes, modeling of a distributed parameter system, in general, and modeling of an isotope separation process in particular, is a task that takes a long time and requires interdisciplinary knowledge. Formulating a model using first-principles knowledge offers a good insight in the physical processes that take place, facilitating later tasks in optimization or process control design. In this paper we have presented in a structured and comprehensive way the modeling approach for a cryogenic ^{13}C distillation plant. Firstly, based on two-film theory we derived the isotopic mass transfer rate followed by the determination of the system of PDEs that govern the evolution of ^{13}C isotope during the separation process. Since the mass transfer device in the case of isotope separation by cryogenic distillation is usually a very long column with a small diameter, a good approximation arises by neglecting the radial diffusion. We continued with the determination of the volumetric overall mass transfer coefficient. Next, we determined the system of PDEs with respect to the desired isotope mole fraction in the enriched phase, resulting in a full nonlinear PDE model. Due to the complexity of this model we derived two additional simplified models, a quasi-linear and, when the isotope concentration achieved during the separation process is low, a linear model. We presented the numerical simulation of these three models for the total-reflux regime followed by the evaluation of the two simplified models with respect to the full nonlinear model. With a maximum relative error of $\pm 0.6\%$ and an average relative error of $\pm 0.3\%$ the linear isotope separation PDE model is a valid modeling approach providing a basis for subsequent studies in modeling and process control.

Future work will involve the simulation of the plant operating in withdrawal regime and the analysis of the effects of the packing (more specifically of the specific interfacial area) over the hold-up, pressure drop, internal flow rates, and production. The condenser decompression, which improves the separation achieved by decreasing the boiling temperature of the cooling agent, will also be treated from both modeling and control points of view. Finally, the effects of the fluctuations of certain plant parameters on the concentration profiles will be analyzed, followed by the isotope separation process control.

Acknowledgements

This paper was supported by the project "Doctoral studies in engineering sciences for developing the knowledge based society-SIDOC" contract no. POSDRU/88/1.5/S/60078, project co-funded from European Social Fund through Sectorial Operational Program Human Resources 2007-2013. The work was supported as well by CNCSIS-UEFISCDI, project number 630 PNII-IDEI code 228/2008.

References

[1] W.G. Mook. Abundance and fractionation of stable isotopes. In W.G. Mook, editor, *Environmental Isotopes in the Hydrological Cycle. Principles and Applications*, volume 1, chapter 3, pages 31–48. UNESCO Publishing, Paris, 2000.

[2] G. Faure and T.M. Mensing. *Isotopes. Principles and Applications.* John Wiley and Sons, Hoboken, third edition, 2005.

[3] R.A. de Vries, M. de Bruin, J.J. Marx, and A. Van de Wiel. Radioisotopic labels for blood cell survival studies: a review. *Nuclear Medicine and Biology*, 20(7):809–817, 1993.

[4] P.A. de Groot. Carbon. In P.A. de Groot, editor, *Handbook of Stable Isotope Analytical Techniques*, volume 2, chapter 4, pages 229–329. Elsevier, Amsterdam, first edition, 2009.

[5] P. Ciais, P.P. Tans, M. Trolier, J.W.C. White, and R.J. Francey. A large norhern hemisphere terrestrial CO_2 sink indicated by the $^{13}C/^{12}C$ ratio of atmospheric CO_2. *Science*, 269(5227):1098–1102, 1995.

[6] J. Bigeleisen. Chemistry of isotopes. *Science*, 147(3657):463–471, 1965.

[7] P.A. de Groot. Isotope separation methods. In P.A. de Groot, editor, *Handbook of Stable Isotope Analytical Techniques*, volume 2, chapter 20, pages 1025–1032. Elsevier, Amsterdam, first edition, 2009.

[8] W.A. Van Hook. Isotope separation. In A. Vértes, S. Nagy, and Z. Klencsár, editors, *Handbook of Nuclear Chemistry*, volume 5, chapter 5, pages 177–211. Kluwer Academic Publishers, Dordrecht, 2003.

[9] H. London. *Separation of Isotopes.* George Newnes Limited, London, 1961.

[10] OECD/Nuclear Energy Agency. *Beneficial Uses and Production of Isotopes.* OECD Publishing, Paris, 2005.

[11] H.C. Urey. The thermodynamic properties of isotopic substances. *Journal of the Chemical Society*, pages 562–581, 1947.

[12] J. Bigeleisen and M.G. Mayer. Calculation of equilibrium constants for isotopic exchange reactions. *The Journal of Chemical Physics*, 15(5):261–267, 1947.

[13] G. Jancso and W.A. Van Hook. Condensed phase isotope effects (especially vapor pressure isotope effects). *Chemical Reviews*, 74(6):689–750, 1974.

[14] K.P. Cohen. *The Theory of Isotope Separation as Applied to the Large-Scale Production of U^{235}*, volume 1B of *National Nuclear Energy Series, Manhattan Project Technical Section, Division III*. McGraw-Hill, New York, first edition, 1951.

[15] B.M. Andreev, E.P. Magomedbekov, A.A. Raitman, M.B. Pozenkevich, Yu.A. Sakharovsky, and A.V. Khoroshilov. *Separation of Isotopes of Biogenic Elements in Two-phase Systems*. Elsevier, Amsterdam, 2007.

[16] B.B. McInteer. Isotope separation by distillation: Design of a carbon-13 plant. *Separation Science and Technology*, 15(3):491–508, 1980.

[17] H.-L. Li, Y.-L. Ju, L.-J. Li, and D.-G. Xu. Separation of isotope ^{13}C using high-performance structured packing. *Chemical Engineering and Processing: Process Intensification*, 49(3):255–261, 2010.

[18] E.-H. Dulf, C. Festila, and F. Dulf. Monitoring and control system of a separation column for ^{13}C enrichment by cryogenic distillation of carbon monoxide. *International Journal of Mathematical Models and Methods in Applied Sciences*, 3(3):196–203, 2009.

[19] E.L. Cussler. *Diffusion. Mass Transfer in Fluid Systems*. Cambridge University Press, Cambridge, third edition, 2009.

[20] C.J. King. *Separation Processes*. McGraw-Hill, New York, second edition, 1980.

[21] S. Skogestad. Dynamics and control of distillation columns: A tutorial introduction. *Chemical Engineering Research and Design*, 75(6):539–562, 1997.

[22] I.J. Halvorsen and S. Skogestad. Theory of Distillation. In I.D. Wilson, E.R. Adlard, M. Cooke, and C.F. Poole, editors, *Encyclopedia of Separation Science*, pages 1117–1134. Academic Press, San Diego, 2000.

[23] S. Skogestad. Plantwide control: the search for the self-optimizing control structure. *Journal of Process Control*, 10(5):487–507, 2000.

[24] M.F. Sågfors and K.V. Waller. Multivariable control of ill-conditioned distillation columns utilizing process knowledge. *Journal of Process Control*, 8(3):197–208, 1998.

[25] H.-X. Li and C. Qi. Modeling of distributed parameter systems for applications - a synthesized review from time-space separation. *Journal of Process Control*, 20(8):891–901, 2010.

[26] C. Qi, H.-T. Zhang, and H.-X. Li. A multi-channel spatio-temporal Hammerstein modeling approach for nonlinear distributed parameter processes. *Journal of Process Control*, 19(1):85–99, 2009.

[27] R. Curtain and K. Morris. Transfer functions of distributed parameter systems: A tutorial. *Automatica*, 45(5):1101–1116, 2009.

[28] L. Debnath. *Nonlinear Partial Differential Equations for Scientists and Engineers*. Birkhäuser, Boston, second edition, 2005.

[29] P.D. Lax and R.D. Richtmyer. Survey of the stability of linear finite difference equations. *Communications on Pure and Applied Mathematics*, 9:267–293, 1956.

[30] T.J. Chung. *Computational Fluid Dynamics*. Cambridge University Press, Cambridge, second edition, 2010.

[31] J.C. Strikwerda. *Finite Difference Schemes and Partial Differential Equations*. SIAM: Society for Industrial and Applied Mathematics, Philadelphia, second edition, 2004.

[32] K.T. Chuang and K. Nandakumar. Tray columns: Design. In I.D. Wilson, E.R. Adlard, M. Cooke, and C.F. Poole, editors, *Encyclopedia of Separation Science*, pages 1135–1140. Academic Press, San Diego, 2000.

[33] L. Klemas and J.A. Bonilla. Packed Columns: Design and Performance. In I.D. Wilson, E.R. Adlard, M. Cooke, and C.F. Poole, editors, *Encyclopedia of Separation Science*, pages 1081–1098. Academic Press, San Diego, 2000.

[34] P. Wankat. *Separation Process Engineering*. Prentice Hall, Upper Saddle River, second edition, 2006.

[35] R.F. Strigle, Jr. *Packed Tower Design and Applications: Random and Structured Packings*. Gulf Publishing Company, Houston, second edition, 1994.

[36] M.R. Fenske. Fractionation of straight-run pennsylvania gasoline. *Industrial and Engineering Chemistry*, 24(5):482–485, 1932.

[37] D. Azbel. *Two-Phase Flows in Chemical Engineering*. Cambridge University Press, Cambridge, 1981.

[38] J.R. Taricska, J.P. Chen, Y.-T. Hung, L.K. Wang, and S.-W. Zou. Surface and spray aeration. In L.K. Wang, N.C. Pereira, and Y-T Hung, editors, *Handbook of Environmental Engineering*, volume 8, pages 157–165. Humana Press, New York, 2009.

[39] F.M. Khoury. *Multistage Separation Processes*, chapter 15, pages 389–410. CRC Press, Boca Raton, third edition, 2005.

[40] J.A. Mandler. Modelling for control analysis and design in complex industrial separation and liquefaction processes. *Journal of Process Control*, 10(2-3):167–175, 2000.

[41] Air Liquide Group. *Physical properties of gases, safety, MSDS, enthalpy, material compatibility, gas liquid equilibrium, density, viscosity, flammability, transport properties*, 2011 (last accessed June 9, 2011). `http://encyclopedia.airliquide.com`.

[42] T.F. Johns. Vapor pressure ratio of $^{12}C^{16}O$ and $^{13}C^{16}O$. *Proceedings of the Physical Society. Section B*, 66(9):808–809, 1953.

[43] J. Niessner and S.M. Hassanizadeh. Modeling kinetic interphase mass transfer for two-phase flow in porous media including fluid-fluid interfacial area. *Transport in Porous Media*, 80(2):329–344, 2009.

[44] A. Tsoularis and J. Wallace. Analysis of logistic growth models. *Mathematical Biosciences*, 179(1):21–55, 2002.

[45] W.H. Young. On the conditions for the reversibility of the order of partial differentiation. *Proceedings Royal Society of Edinburgh*, 29:136–164, 1908-1909.

[46] H.-X. Li, C. Qi, and Y. Yu. A spatio-temporal Volterra modeling approach for a class of distributed industrial processes. *Journal of Process Control*, 19(7):1126–1142, 2009.

[47] D.S. Burnett. *Finite Element Analysis: from Concepts to Applications*. Addison-Wesley, Reading, 1987.

[48] J.H. Mathews and K.D. Fink. *Numerical Methods using MATLAB*. Prentice Hall, Upper Saddle River, third edition, 1999.

[49] S. Jacob, S. Kasthurirengan, and R. Karunanithi. Investigations into the thermal performance of multilayer insulation (300-77 K) Part 1: Calorimetric studies. *Cryogenics*, 32(12):1137–1146, 1992.

[50] S. Jacob, S. Kasthurirengan, and R. Karunanithi. Investigations into the thermal performance of multilayer insulation (300-77 K) Part 2: Thermal analysis. *Cryogenics*, 32(12):1147–1153, 1992.